Chapter 3

SELF-ASSEMBLY OF SYMMETRIC BRUSH BLOCK COPOLYMERS

Reproduced in part with permission from:
Gu, W.; Huh, J.; Hong, S. W.; Sveinbjornsson, B. R.; Park, C.; Grubbs, R. H.; Russell, T. P. *ACS Nano* **2013**, *7*, 2551-2558.
Hong, S. W.; Gu, W.; Huh, J.; Sveinbjornsson, B. R.; Jeong, G.; Grubbs, R. H.; Russell, T. P. *ACS Nano* **2013**, *7*, 9684-9692

ABSTRACT

Self-assembled structures of brush block copolymers (BCPs) with polylactide (PLA) and polystyrene (PS) side chains were studied in bulk and thin films. The polynorbornene-backbone-based brush BCPs containing approximately equal volume fractions of each block self-assembled into highly ordered lamellae, with domain spacing ranging from 20 to 240 nm by varying molecular weight of the backbone, as revealed by small-angle X-ray scattering (SAXS). The domain size increased approximately linearly with backbone length, which indicated an extended conformation of the backbone in the ordered state. The domain sizes of samples in thin films were found to be consistently larger than the corresponding domain sizes in bulk. The thin film samples were also found to orient perpendicularly to the silica substrate, without modification to the underlying substrate. *In situ* SAXS measurements suggested that the brush BCPs self-assemble in an extremely fast manner that could be attributed to reduced number of entanglements between chains.

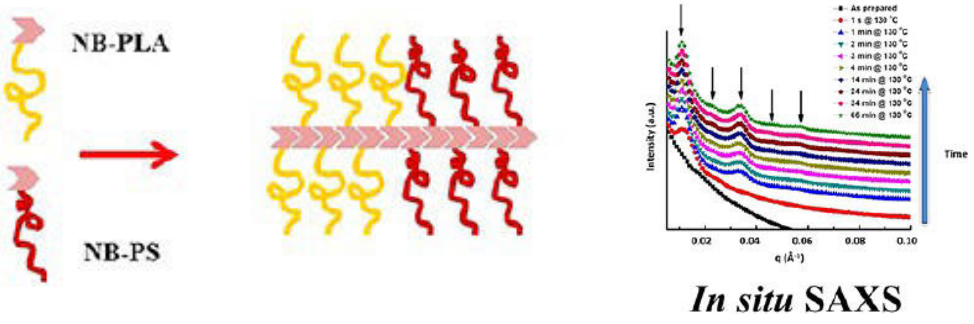

INTRODUCTION

Well-defined, periodic morphologies with features from the nanometer to hundreds of nanometer size scale have received considerable attention, because they can be used as templates and scaffolds for the fabrication of nanodots, nanowires, magnetic storage media, semiconductors, and optical devices, including polarizers and photonic band gap materials.[1–14] The self-assembly of block copolymers (BCPs) is proving to be one of the more promising bottom-up approaches to generating such morphologies in a cost-effective, robust, and scalable manner.[10,12,15–23] While there has been a tremendous drive to continually reduce the size scale of the features (with 3 nm feature sizes being the smallest achieved to date[20]), there are still numerous applications, such as polarizers and photonic bandgap materials, that require feature sizes on the scale of hundreds of nanometers. The use of self-assembly or directed self-assembly of BCPs could significantly reduce the number of steps required to generate features of this size, and therefore lead to a substantial cost savings. Since the period (pitch) of BCP morphologies and the dimensions of microdomains scale approximately with the 2/3 power of the molecular weight (for BCPs comprised of flexible chains in the strong segregation limit), achieving large scale feature requires the use of exceptionally high molecular weight (MW) BCPs. There has not been much, if any, success in using high MW BCPs to achieve large-scale features, because the diffusion of the polymers is exceptionally slow,[24] which significantly retards the self-assembly of the BCPs into highly ordered arrays of microdomains, as well as the elimination of defects in the resultant morphologies. Supercritical carbon dioxide (CO_2) at elevated temperatures has been used to swell BCPs, enhance the diffusion, and to order the BCP microdomains on the 0.1 μm size scale.[25] This still requires prolonged annealing times, and care must be taken to prevent void formation when the CO_2 is removed. Ryu and co-workers reported that polystyrene-*b*-poly(methyl methacrylate) (PS-*b*-PMMA) lamellae with large periods are obtained by solvent annealing sequentially combined with thermal annealing, but this requires multiple steps.[26] In the development of BCPs for photonic bandgap applications, Thomas and co-workers used conventional BCPs and polyelectrolyte-based BCPs with solvents or homopolymer/small molecule additives to achieve periodicities on the scale of 100 nm and larger.[27–29] However, achieving highly ordered structures on the 0.25 μm size scale or larger in an easy and rapid manner with BCPs has been exceedingly difficult.

To the best of our knowledge, there have been relatively few efforts to fabricate and control the ordering and orientation of periodic nanostructures using brush polymers.[30,31] However, the promising results discussed in *Chapter 2*, where we were able to obtain NIR-reflecting photonic bandgap materials rapidly using the self-assembly of brush BCPs, were a motivation for pursuing further studies on the self-assembly of the brush BCP system. Here we discuss a study on the self-assembly of these brush BCPs, both in the bulk state and in thin film. We also report the scaling relationship between the degree of polymerization (DP) of brush polymers and the domain spacing observed from the self-assembled brush polymers for a few different side chain sizes.

SYNTHESIS OF BRUSH BCPs

The brush BCPs were synthesized using a ruthenium-catalyzed ring-opening metathesis polymerization (ROMP) of polylactide (PLA) and polystyrene (PS) based macromonomers (MMs) in an analogous way to the brush BCPs discussed in *Chapter 2* (**Scheme 3-1**). Four separate series were synthesized with side chains ranging from 2.4 × 10^3 g/mol to 9.9 × 10^3 g/mol and total DP of 25 and up to 869 MM units. **Table 3-1** shows the sample codes and characteristics of the brush BCPs used in this study. In the sample code form $[g\text{-}S_x]_p\text{-}b\text{-}[g\text{-}LA_y]_q$, the subscripts *x* and *y* are the molecular weights of the side chains of each type (in units of one thousand), and subscripts *p* and *q* represent the degree of polymerization of each brush block.

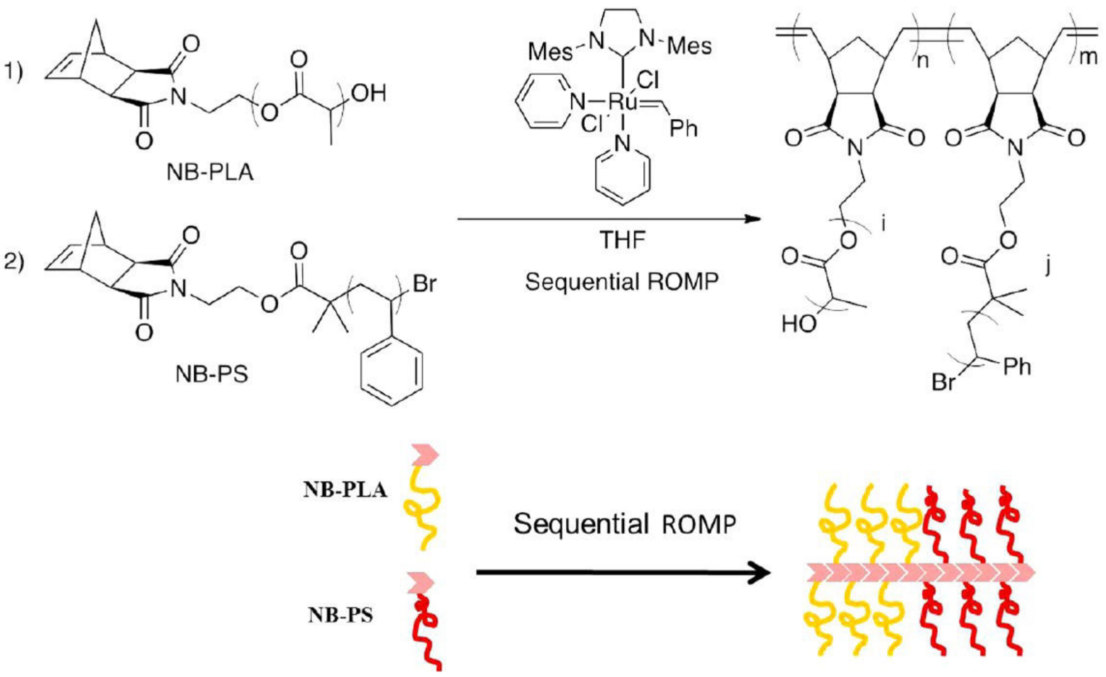

Scheme 3-1. General synthetic route and schematic diagram of brush block copolymers.

Table 3-1. Sample codes and characteristics of symmetric brush block copolymers.

Group	Sample codes	Total M_n [a] (× 10^3 g/mol)	Total DP [b]	L (nm)	
				Bulk [c]	Thin Films [d]
I	$[g\text{-S}_{2.4}]_{19}\text{-}b\text{-}[g\text{-LA}_{2.4}]_{25}$	105	44	19.2	22.0
	$[g\text{-S}_{2.4}]_{35}\text{-}b\text{-}[g\text{-LA}_{2.4}]_{43}$	186	78	33.6	40.0
	$[g\text{-S}_{2.4}]_{51}\text{-}b\text{-}[g\text{-LA}_{2.4}]_{67}$	281	118	54.6	61.0
	$[g\text{-S}_{2.4}]_{98}\text{-}b\text{-}[g\text{-LA}_{2.4}]_{124}$	529	222	91.0	116.0
	$[g\text{-S}_{2.4}]_{189}\text{-}b\text{-}[g\text{-LA}_{2.4}]_{233}$	1007	422	157	215.1
	$[g\text{-S}_{2.4}]_{259}\text{-}b\text{-}[g\text{-LA}_{2.4}]_{381}$	1525	640	[e]	[f]
II	$[g\text{-S}_{4.3}]_{11}\text{-}b\text{-}[g\text{-LA}_{4.5}]_{14}$	104	25	19.8	20.9
	$[g\text{-S}_{4.3}]_{19}\text{-}b\text{-}[g\text{-LA}_{4.5}]_{25}$	192	44	31.2	31.1
	$[g\text{-S}_{4.3}]_{32}\text{-}b\text{-}[g\text{-LA}_{4.5}]_{42}$	320	74	43.9	45.2
	$[g\text{-S}_{4.3}]_{42}\text{-}b\text{-}[g\text{-LA}_{4.5}]_{58}$	432	100	58.7	62.2
	$[g\text{-S}_{4.3}]_{93}\text{-}b\text{-}[g\text{-LA}_{4.5}]_{128}$	954	221	102.9	149.5
	$[g\text{-S}_{4.3}]_{206}\text{-}b\text{-}[g\text{-LA}_{4.5}]_{278}$	2089	484	235[g]	[f]
III	$[g\text{-S}_{5.8}]_{13}\text{-}b\text{-}[g\text{-LA}_{6.1}]_{11}$	140	24	-	-
	$[g\text{-S}_{5.8}]_{30}\text{-}b\text{-}[g\text{-LA}_{6.1}]_{25}$	326	55	-	-
	$[g\text{-S}_{5.8}]_{51}\text{-}b\text{-}[g\text{-LA}_{6.1}]_{46}$	574	97	-	-
	$[g\text{-S}_{5.8}]_{101}\text{-}b\text{-}[g\text{-LA}_{6.1}]_{95}$	1166	196	-	-
	$[g\text{-S}_{5.8}]_{244}\text{-}b\text{-}[g\text{-LA}_{6.1}]_{209}$	2682	452	-	-
	$[g\text{-S}_{5.8}]_{471}\text{-}b\text{-}[g\text{-LA}_{6.1}]_{397}$	5150	869	-	-
IV	$[g\text{-S}_{9.9}]_{13}\text{-}b\text{-}[g\text{-LA}_{9.5}]_{10}$	220	23	-	-
	$[g\text{-S}_{9.9}]_{33}\text{-}b\text{-}[g\text{-LA}_{9.5}]_{25}$	572	59	-	-
	$[g\text{-S}_{9.9}]_{62}\text{-}b\text{-}[g\text{-LA}_{9.5}]_{48}$	1070	110	-	-
	$[g\text{-S}_{9.9}]_{165}\text{-}b\text{-}[g\text{-LA}_{9.5}]_{127}$	2836	292	-	-
	$[g\text{-S}_{9.9}]_{294}\text{-}b\text{-}[g\text{-LA}_{9.5}]_{180}$	4621	474	-	-

[a] Determined by THF GPC using RI and MALLS detectors. [b] Degree of polymerization determined by ^{1}H NMR and THF GPC (as described in *Chapter 2*). [c] The domain spacing L_0 is calculated from the corresponding first-order peak position of the 1-D SAXS profiles ($L_0 = 2\pi/q^*$) unless noted. [d] Center-to-center distance between microdomains determined by GI-SAXS analysis. [e] Peaks are absent during the given experimental condition. [f] Microdomains spacing by GI-SAXS analysis. [g] The first peak value is derived from the higher-order peaks.

SELF-ASSEMBLY OF BRUSH BCPs IN BULK

Bulk samples were prepared in aluminum washers, which were sandwiched by Kapton films and kept in a vacuum oven for 12 hours or longer to achieve thermal equilibrium before SAXS measurements were taken. Circular patterns were observed in the 2D SAXS results from bulk samples of group I and group II (**Figure 3-1 and Figure 3-2**) Samples with low MW in each series showed distinguishable multiple ring patterns (**Figure 3-1 A-D and Figure 3-2 A-E**), indicating that well-ordered microphase structures were formed isotropically in the bulk state. Meanwhile, the domain spacing of high MW samples (**Figure 3-1 E-F, Figure 3-2 F**) may have been too large and beyond the limit of SAXS, or microdomains may not have been as well-ordered. Profiles of the scattering intensity *versus* scattering vector were also generated from **Figure 3-1** and **Figure 3-2**, and are shown in **Figure 3-3**. A systematic decrease in q^*, the scattering vector of the first-order reflection, was observed from low MW brush BCP to high MW brush BCP, indicating the anticipated increase of the domain spacing ranging from 19.2 to 235 nm (**Table 3-1**). Strong reflections were also seen at integral multiples of q^* in most cases, indicating the lamellar nature of the microdomains with long-range lateral ordering, as expected due to the near symmetric volume fractions of the PS and PLA segments.

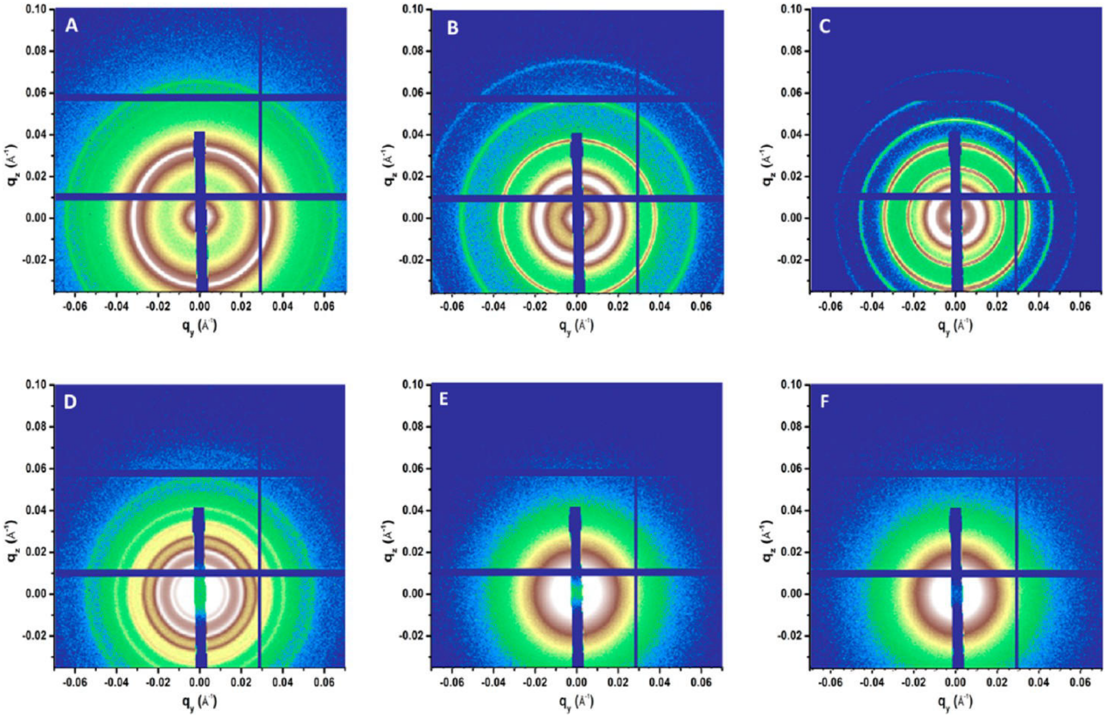

Figure 3-1. Representative 2D SAXS patterns for (A) [*g*-S$_{2.4k}$]$_{19}$-*b*-[*g*-LA$_{2.4k}$]$_{25}$; (B) [*g*-S$_{2.4k}$]$_{35}$-*b*-[*g*-LA$_{2.4k}$]$_{43}$; (C) [*g*-S$_{2.4k}$]$_{51}$-*b*-[*g*-LA$_{2.4k}$]$_{67}$; (D) [*g*-S$_{2.4k}$]$_{98}$-*b*-[*g*-LA$_{2.4k}$]$_{124}$; (E) [*g*-S$_{2.4k}$]$_{189}$-*b*-[*g*-LA$_{2.4k}$]$_{233}$; and (F) [*g*-S$_{2.4k}$]$_{259}$-*b*-[*g*-LA$_{2.4k}$]$_{381}$.

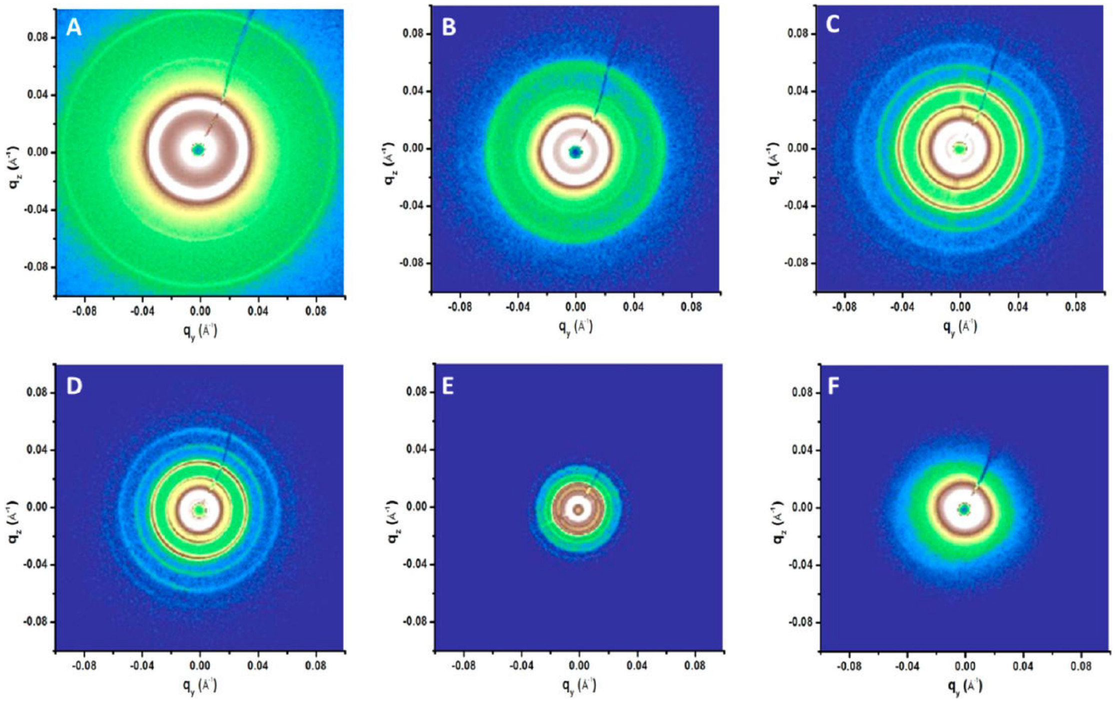

Figure 3-2. Representative 2D SAXS patterns for (A) [*g*-$S_{4.3k}$]$_{11}$-*b*-[*g*-$LA_{4.5k}$]$_{14}$; (B) [*g*-$S_{4.3k}$]$_{19}$-*b*-[*g*-$LA_{4.5k}$]$_{25}$; (C) [*g*-$S_{4.3k}$]$_{32}$-*b*-[*g*-$LA_{4.5k}$]$_{42}$; (D) [*g*-$S_{4.3k}$]$_{42}$-*b*-[*g*-$LA_{4.5k}$]$_{58}$; (E) [*g*-$S_{4.3k}$]$_{93}$-*b*-[*g*-$LA_{4.5k}$]$_{128}$; (F) [*g*-$S_{4.3k}$]$_{206}$-*b*-[*g*-$LA_{4.5k}$]$_{278}$.

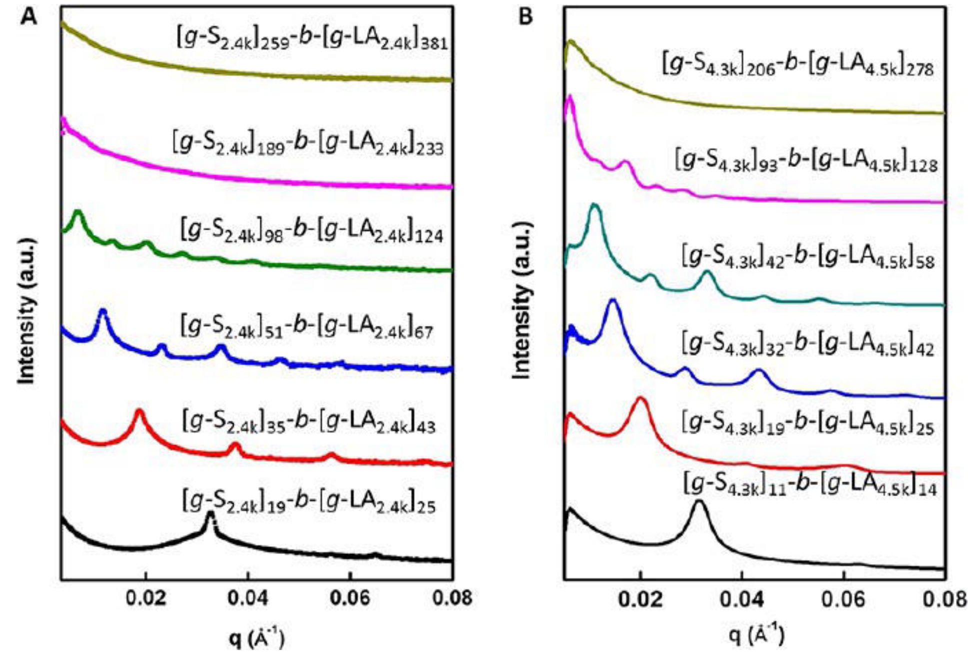

Figure 3-3. One-dimensional SAXS profiles calculated from the 2-D SAXS patterns in Figure 3-1 and Figure 3-2, respectively. (A) Group I. (B) Group II. Profile curves were offset for clarity

To further analyze the relationship between the measured domain spacing, L_0, and DP of the backbone, L_0 was plotted against total DP in a log-log plot (**Figure 3-4**). The exponents v in the scaling form $L_0 \sim \mathrm{DP}^v$ for both cases were determined from the slope: $v = 0.84$ for group I, and $v = 0.91$ for group II. Both values are greater than the power law index determined in the SSL region, which is 2/3, and were also even greater than the greatest value previously reported, to the best of our knowledge, for a PS-*b*-PLA based BCP system (0.81).[32,33] This suggests that the backbones of brush BCPs are highly stretched as the PS and PLA side chains are segregated from each other, since the stretching of the backbone decreases the PS/PLA interfacial area per unit volume. Since group II brush BCPs have longer side chains compared with group I, steric hindrance may make the backbone more rigid, and thus cause the v value to be even larger.

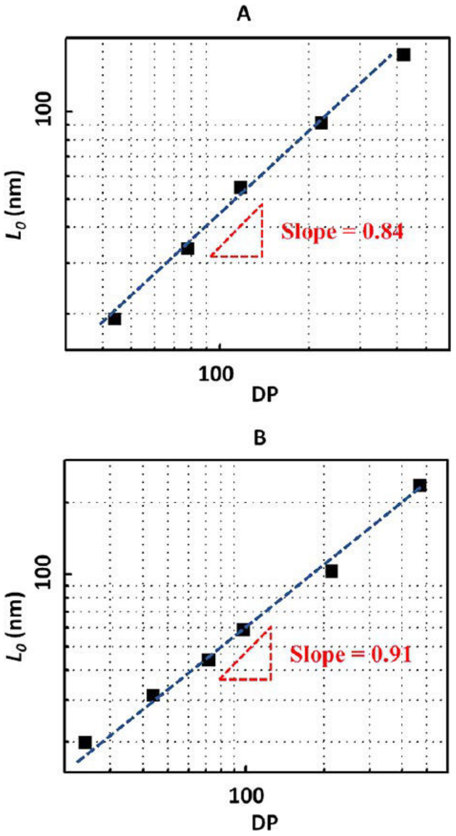

Figure 3-4. Scaling law between L_0 and DP. (A) Group I. (B) Group II.

Samples from group III were also analyzed via SAXS, and the results used to plot L_0 against the DP (**Figure 3-5**). Interestingly, the v value for this series was lower than that for group II even though it had longer side chains. Attempts were also made at analogous analysis of samples from group IV with limited success so far. This suggests that as the side chains grow longer, it may become increasingly difficult to obtain well-ordered microdomains, at least with the annealing techniques used here. Therefore, there may be an optimal side chain length for these brush polymers to give the highest *v* value while being able to self-assemble into well-ordered microdomains in the bulk.

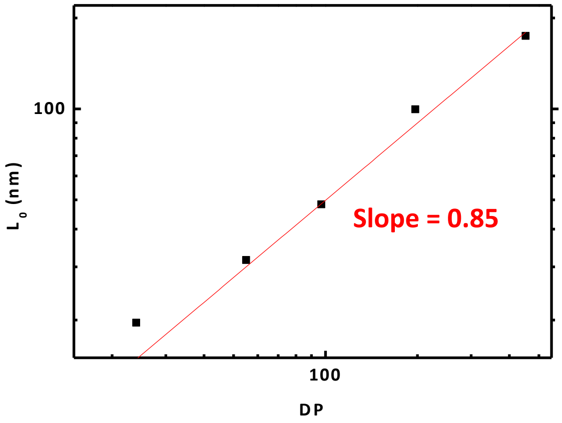

Figure 3-5. Scaling law between L_0 and DP for group III.

SELF-ASSEMBLY OF BRUSH BCPs IN THIN-FILMS

Thin films of brush BCPs were prepared on silicon substrates and, to effectively induce well-developed nanostructures, thin films were then solvent-annealed using either pure tetrahydrofuran (THF) or a mixture of solvents, tetrahydrofuran/chlorobenzene (THF/CBz), by which interfacial interactions were mediated. Scanning force microscopy (SFM) and grazing incidence small angle X-ray scattering (GI-SAXS) were used to characterize thin films of brush BCPs.

Interestingly, when thin films of $[g\text{-}S_{2.4}]_{189}\text{-}b\text{-}[g\text{-}LA_{2.4}]_{233}$ (film thickness was measured to be 47nm by ellipsometry), which has an extremely high MW of 1007×10^3 g/mol, were solvent-annealed with THF/CBz, well-developed lamellar microdomains oriented perpendicular to the substrate were obtained within a relatively short solvent-annealing time, as shown in **Figure 3-6**. From the SFM analysis, *L* of $[g\text{-}S_{2.4}]_{189}\text{-}b\text{-}[g\text{-}LA_{2.4}]_{233}$ is measured to be 228.5 nm. The microphase separation of the brush BCP is rapid, in comparison to conventional BCPs. This is due to the fact that the brush BCP backbone is more rigid than that of a conventional flexible BCP caused by steric hindrance, and consequently there is a reduction in the number of chain-entanglements when compared to analogous linear BCPs with the same MW. Therefore, even ultrahigh MW brush BCPs will rapidly self-assemble into well-ordered microphase-separated morphologies that have extremely large feature sizes. Additional SFM images of lamellar-forming $[g\text{-S}_{2.4}]_p\text{-}b\text{-}[g\text{-LA}_{2.4}]_q$ and $[g\text{-S}_{4.3}]_p\text{-}b\text{-}[g\text{-LA}_{4.5}]_q$ series are shown in **Figure 3-7** and **Figure 3-8**. It was also remarkable that lamellar microdomains formed by those brush BCPs were oriented perpendicular to the substrate without any need of surface modification. As shown in **Scheme 3-2**, the conventional linear BCPs will generally form a layer-by-layer structure, due to the surface energy difference between two blocks and preferential interactions between one block and the substrate or air interface. However, for the brush BCPs used in this study, lamellar microdomains were oriented perpendicular to the substrate, the origin of which was attributed to the entropy gain caused by the unique chain architecture.

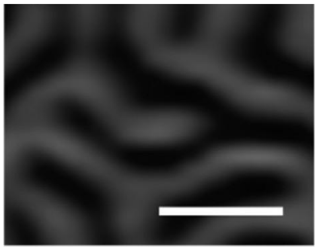

Figure 3-6. SFM height image of solvent-annealed thin film of $[g\text{-S}_{2.4}]_{189}\text{-}b\text{-}[g\text{-LA}_{2.4}]_{233}$ on Si substrate. The solvent annealing time was 10 hours. The scale bar is 400 nm.

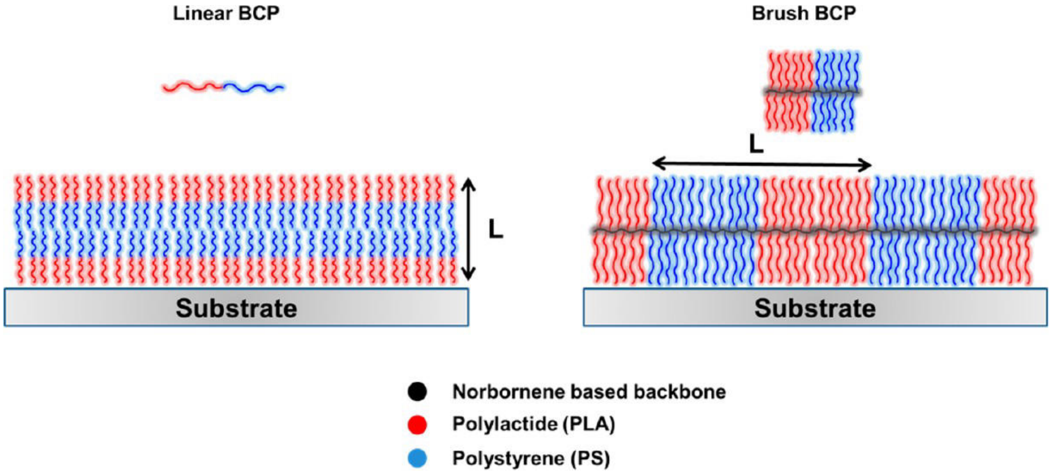

Scheme 3-2. Schematic of lamellar microdomains oriented parallel (left) or perpendicular (right) to the substrate from the self-assembly of linear BCP or brush BCP.

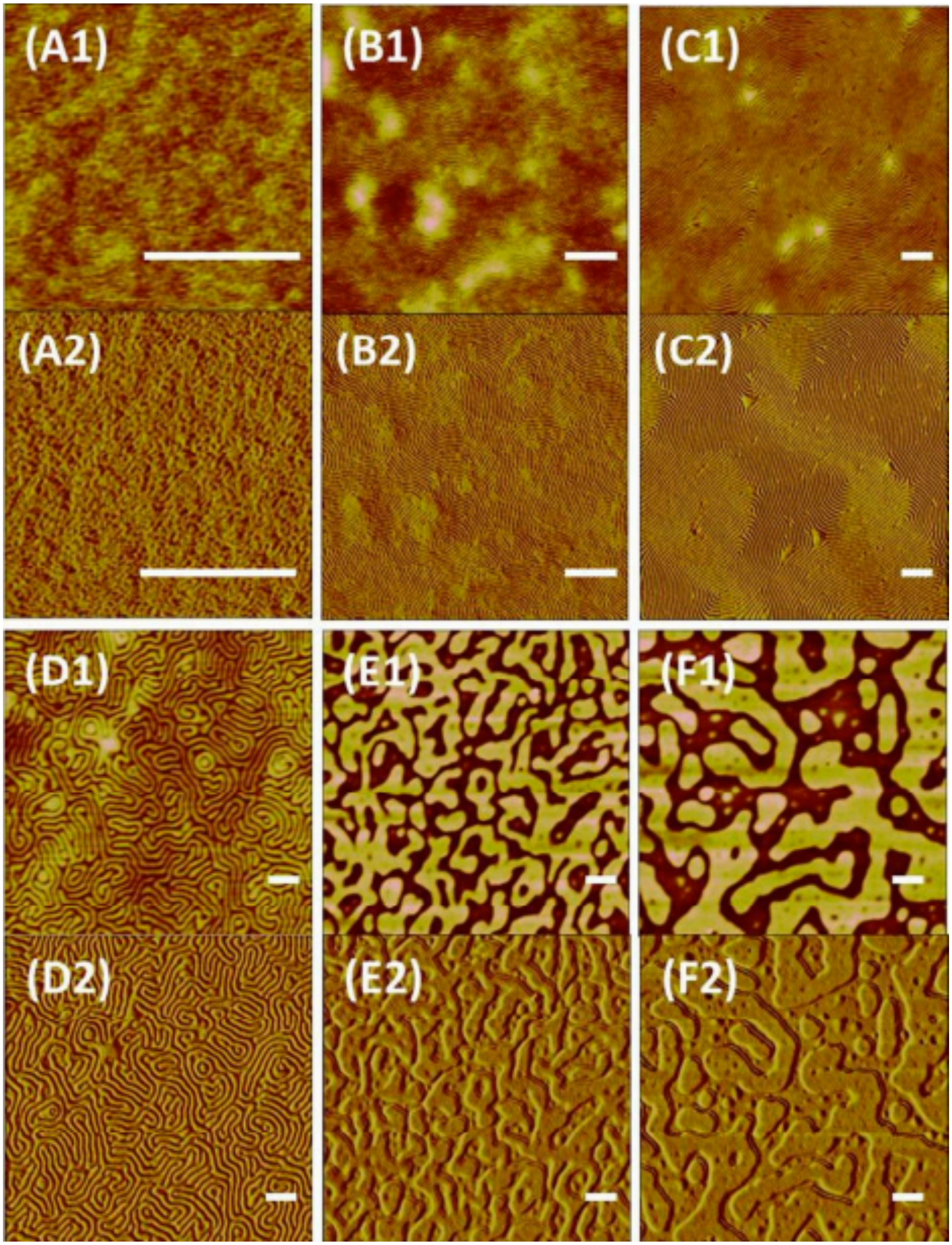

Figure 3-7. SFM height (A1-F1) and phase (A2-F2) images of solvent annealed thin films of $[g\text{-}S_{2.4}]_{19}$-*b*-$[g\text{-}LA_{2.4}]_{25}$, $[g\text{-}S_{2.4}]_{35}$-*b*-$[g\text{-}LA_{2.4}]_{43}$, $[g\text{-}S_{2.4}]_{51}$-*b*-$[g\text{-}LA_{2.4}]_{67}$, $[g\text{-}S_{2.4}]_{98}$-*b*-$[g\text{-}LA_{2.4}]_{124}$, $[g\text{-}S_{2.4}]_{189}$-*b*-$[g\text{-}LA_{2.4}]_{233}$, and $[g\text{-}S_{2.4}]_{259}$-*b*-$[g\text{-}LA_{2.4}]_{381}$, respectively. Scale bars: 500 nm.

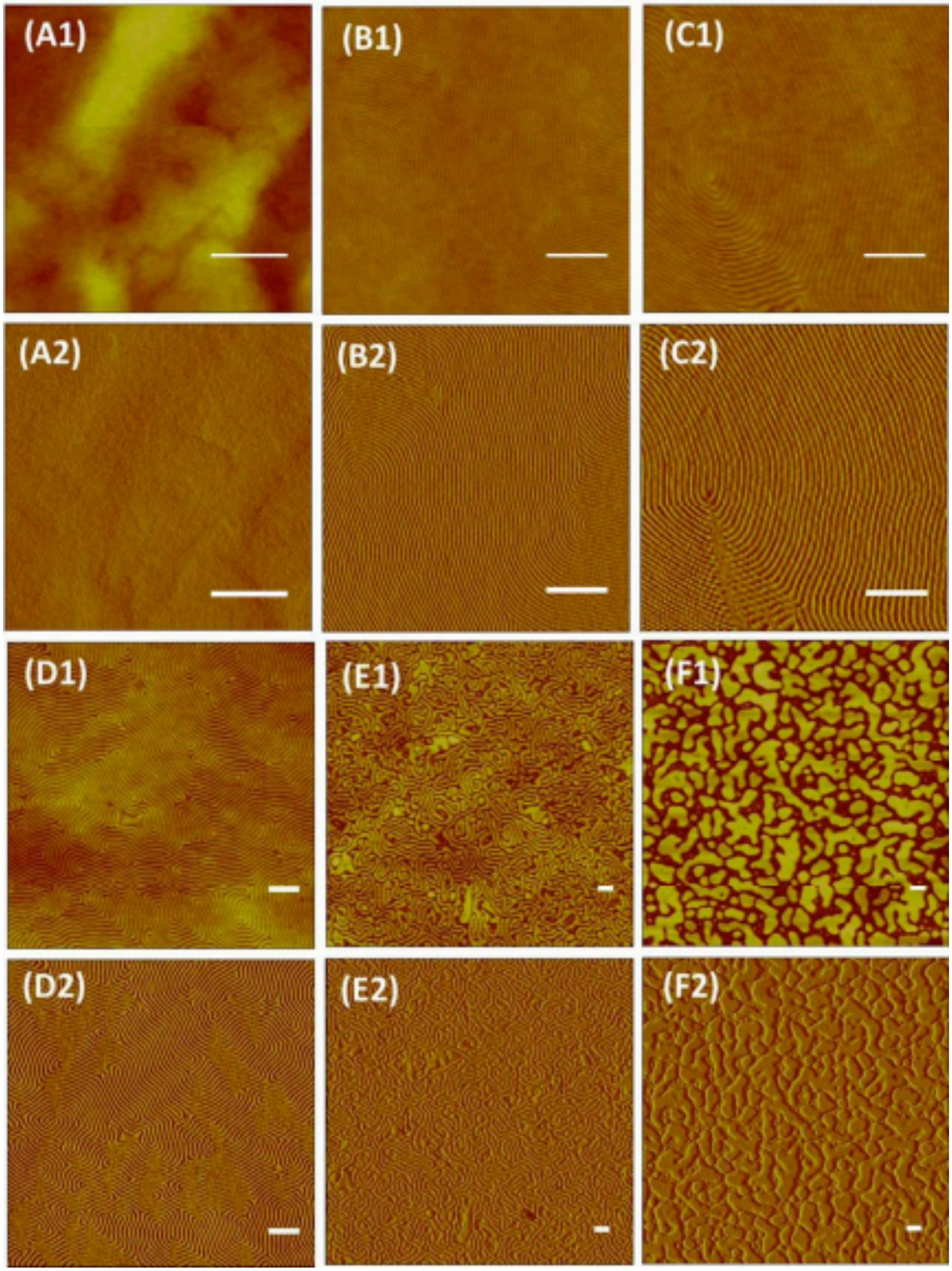

Figure 3-8. SFM height (A1-F1) and phase (A2-F2) images of solvent annealed thin films of $[g\text{-}S_{4.3}]_{11}$-*b*-$[g\text{-}LA_{4.5}]_{14}$, $[g\text{-}S_{4.3}]_{19}$-*b*-$[g\text{-}LA_{4.5}]_{25}$, $[g\text{-}S_{4.3}]_{32}$-*b*-$[g\text{-}LA_{4.5}]_{42}$, $[g\text{-}S_{4.3}]_{42}$-*b*-$[g\text{-}LA_{4.5}]_{58}$, $[g\text{-}S_{4.3}]_{93}$-*b*-$[g\text{-}LA_{4.5}]_{128}$, and $[g\text{-}S_{4.3}]_{206}$-*b*-$[g\text{-}LA_{4.5}]_{278}$, respectively. Scale bars: 500 nm.

The fact that no special steps were taken to modify the substrate in order to control interfacial interactions,[34–37] and the orientation of the lamellar microdomains normal to the substrate, even with solvent annealing, was surprising, because PLA has strongly preferential interactions with the oxide layer on the silicon substrate, and the orientation found requires that the PS block be in contact with the substrate. Consequently, the orientation of the lamellar microdomains normal to the substrate may arise from the screening of the interactions of the blocks with the substrate, coupled with more favored parallel alignment of the sterically hindered, rigid blocks at the polymer/substrate interface, which again is an entropic-type of preferred chain orientation. Unlike linear BCPs, the many chain ends of the side chains attached to the backbone would preferentially segregate to the surface and substrate interfaces. This orientation allows the microphase-separated brush BCPs to have more conformational degrees of freedom, in comparison to the case where microdomains of brush BCPs are oriented parallel to the substrate.

The GI-SAXS studies on the group I and group II series are shown in **Figure 3-9**. From the first order reflection in the GI-SAXS, the period, *L*, was determined. **Figure 3-10** shows *L* as a function of DP for both series of brush BCPs (results summarized in **Table 3-1**). From a regression analysis of the data it was found that $L \propto \mathrm{DP}^{0.99}$ for group I, and $L \propto \mathrm{DP}^{1.03}$ for group II. The slight increase in the exponent as the side chain length increases, and the apparent saturation, with a further increase in the side chain molecular weight, arises from the entropic penalty associated with the packing of the side chains. It is evident, though, that the backbone chain is highly stretched, regardless of MW of the side chain, and only the extended contour length of the main chain dictates *L*. Again, it should be noted that the exponent for the brush BCPs is much larger than that for flexible BCPs in the strong segregation regime,[15] where $L \propto \mathrm{DP}^{2/3}$.

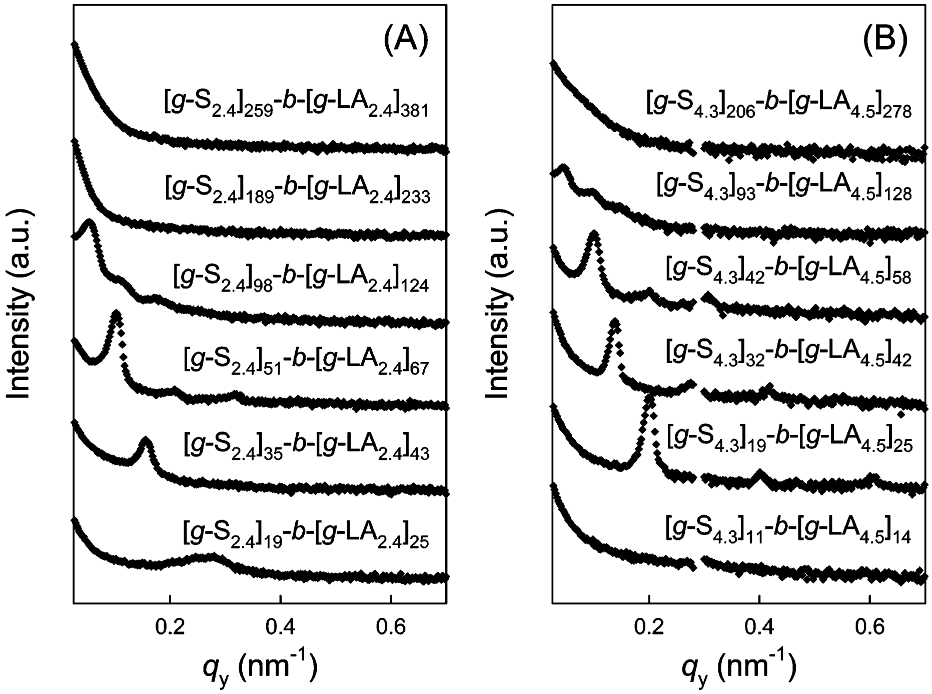

Figure 3-9. GI-SAXS patterns from Brush BCP thin films having different side chains: (A) MW of PS side chain is 2.4 × 10^3 g/mol and MW of PLA side chain is 2.4 × 10^3 g/mol; (B) MW of PS side chain is 4.3 × 10^3 g/mol and MW of PLA side chain is 4.5 × 10^3 g/mol. Film thicknesses, as measured by ellipsometry, ranged from 38 to 63 nm.

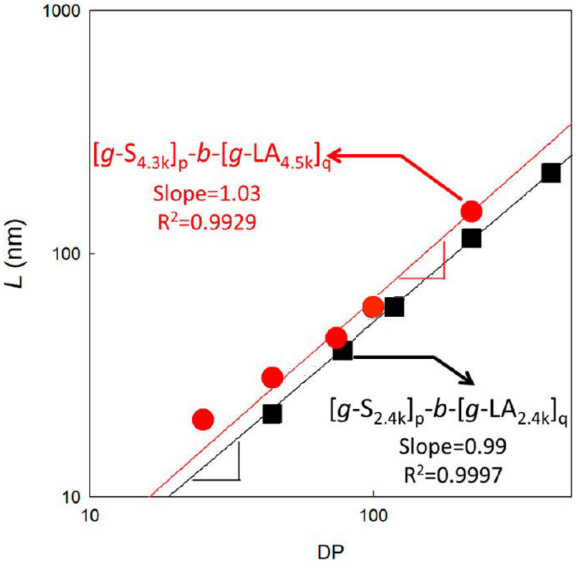

Figure 3-10. Plot of the period (*L*) as a function of degree of polymerization (DP) of the backbone for brush BCPs with different side chains (2.5 × 10^3 g/mol for PS and 2.5 × 10^3 g/mol for PLA (black square), 4.3 × 10^3 g/mol for PS and 4.5 × 10^3 g/mol for PLA (red circle)).

As discussed in the previous section, similar results were found in the case of the thermally annealed bulk samples of brush BCPs. In particular, the domain spacing found with solvent annealing is consistently larger than that for thermal annealing, because the swollen domain spacing during solvent annealing is kinetically trapped during the evaporation of the solvent vapor after the sample is removed from the annealing jar. Consequently, the exponents in the bulk state (thermal annealing) are smaller than that in film state (solvent annealing), indicating that the backbone chains are more stretched in solvent-annealed films.

Thin films made from the highest MW brush BCPs showed a very curious surface topography after solvent annealing for 2 hours in THF vapor. The film thickness in **Figure 3-11** was determined by ellipsometry to be 60, 63, and 65 nm, respectively. A uniform height difference between the two microdomains was observed in **Figure 3-11A** and **B**, where representative thin films of brush BCPs with the same side chain MWs, but with different DPs of the backbone ($[g\text{-}S_{2.4}]_{189}\text{-}b\text{-}[g\text{-}LA_{2.4}]_{233}$ and $[g\text{-}S_{2.4}]_{259}\text{-}b\text{-}[g\text{-}LA_{2.4}]_{381}$), were shown. Analysis of the surface topography shows that terraces formed on the surface, with a step height of only 9 nm for both brush BCPs. This is far less than the step height, *L*, arising from incommensurability between the film thickness and *L*, when the microdomains orient parallel to the surface.[38,39] When the molecular weight of the side chains was increased, as shown in **Figure 3-11C** ($[g\text{-}S_{4.3}]_{206}\text{-}b\text{-}[g\text{-}LA_{4.5}]_{278}$), the step changed to being 13 nm. These values correspond roughly to the diameters of the brushes, and suggest that there is a single layer of the brush BCP covering the surface of the film. X-ray photon spectroscopy (XPS) was used to characterize the composition of the surface of the films (**Table 3-2**), which, from an atomic concentration analysis, suggests that the PS-brush block is preferentially covering the surface. This would be consistent with the lower surface energy of the PS-brush block, but also suggests that the brush BCP must assume a rather unusual bent configuration at the surface in order to minimize the surface energy. The exact nature of this configuration is unknown, at present, and is under further study. It is also noted that the difference in film thickness and solvent annealing time can have a significant influence on final morphologies; for example, both **Figure 3-6** and **Figure 3-11A** are from the same sample, but behave differently.

Table 3-2. Carbon:Oxygen Atomic Concentration (According to C 1s and O 1s Peaks in XPS Spectrscopy).

Sample	15°	75°
$[g\text{-}S_{2.4}]_{189}\text{-}b\text{-}[g\text{-}LA_{2.4}]_{233}$	80.2:11.5	89.5:7.2
$[g\text{-}S_{2.4}]_{259}\text{-}b\text{-}[g\text{-}LA_{2.4}]_{381}$	70.2:24.9	73.9:25
$[g\text{-}S_{4.3}]_{206}\text{-}b\text{-}[g\text{-}LA_{4.5}]_{278}$	79.2:20.8	78.8:21.2

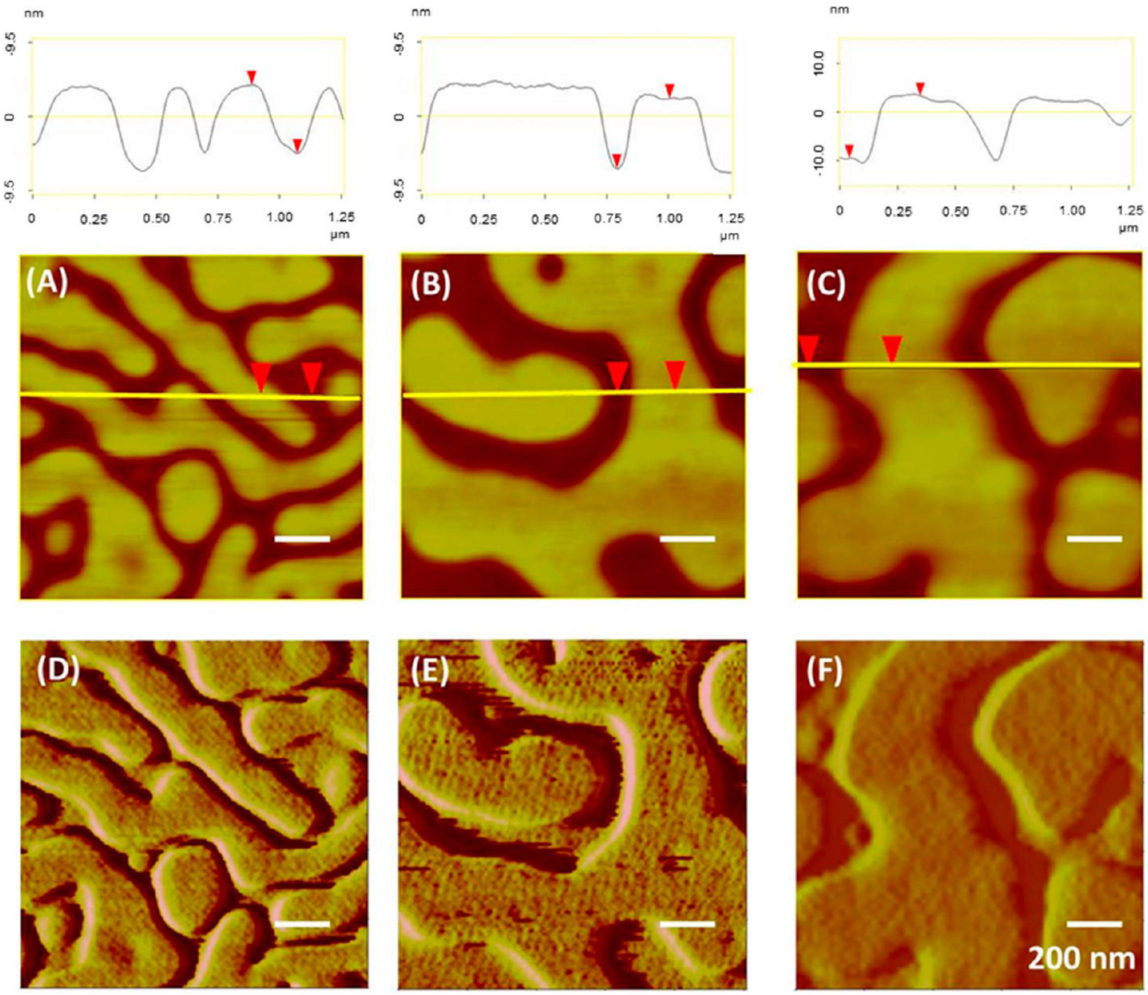

Figure 3-11. SFM height (A-C) and phase (D-F) images obtained from thin films of $[g\text{-}S_{2.4}]_{189}\text{-}b\text{-}[g\text{-}LA_{2.4}]_{233}$, $[g\text{-}S_{2.4}]_{259}\text{-}b\text{-}[g\text{-}LA_{2.4}]_{381}$, and $[g\text{-}S_{4.3}]_{206}\text{-}b\text{-}[g\text{-}LA_{4.5}]_{278}$ on Si substrates, respectively. The plots above SFM images are cross sectional analysis of the corresponding height images below.

FAST KINETICS OF SELF-ASSEMBLY IN THE BULK

Polymer entanglement causes a kinetic barrier for polymers to self-assemble, thus leading to a slow kinetic process of the self-assembly. As the polymers grow bigger, entanglement can have an increased effect on the self-assembly process. Brush polymers have, on the other hand, been reported to show non-entangled dynamics at the high MW regime up to several thousand kilodaltons,[40] which allows us to expect a more rapid self-assembly process even for the ultra-high MW (hundreds to thousands of kilodaltons, as indicated in **Table 3-1**) of brush BCPs. This inspired us to take a closer look at the unique properties of those brush BCPs and their self-assembly behavior in the bulk state. *In situ* SAXS was used to monitor the kinetics of the self-assembly process. **Figure 3-12** shows representative examples of samples [g-S$_{2.4}$]$_{35}$-b-[g-LA$_{2.4}$]$_{43}$, [g-S$_{2.4}$]$_{51}$-b-[g-LA$_{2.4}$]$_{67}$, and [g-S$_{2.4}$]$_{98}$-b-[g-LA$_{2.4}$]$_{124}$. For instance, in **Figures 3-12B**, the initial state, as indicated by the bottom black curve, did not show any distinct peak and exhibited a gradual decrease in intensity, suggesting that chains of brush BCPs were in random arrangements. A measurement was taken immediately (1 s, red curve) once the temperature was increased to 130 °C and a primary peak at ~ 0.012 Å^{-1} appeared. This implies that a characteristic distance was developed, although it was not too well-defined due to its broad shape. Upon longer annealing time, the primary scattering wavevector q* shifted a little bit to smaller q value (0.011 Å), and higher-order reflections were profoundly enhanced at integral multiples of q*, evidence of improvement in lateral order of lamellar structures. Notably, the low MW brush BCP (**Figure 3-12A**) self-assembled much more rapidly (~5 minutes) in comparison to the high MW (**Figure 3-12C**, ~1 hour) brush BCP. It is understandable that low MW brush BCPs have less entanglement between chains, and thus the mobility is higher. Nevertheless, these results show that well-ordered lamellar structures were formed within an hour for all of the samples shown.

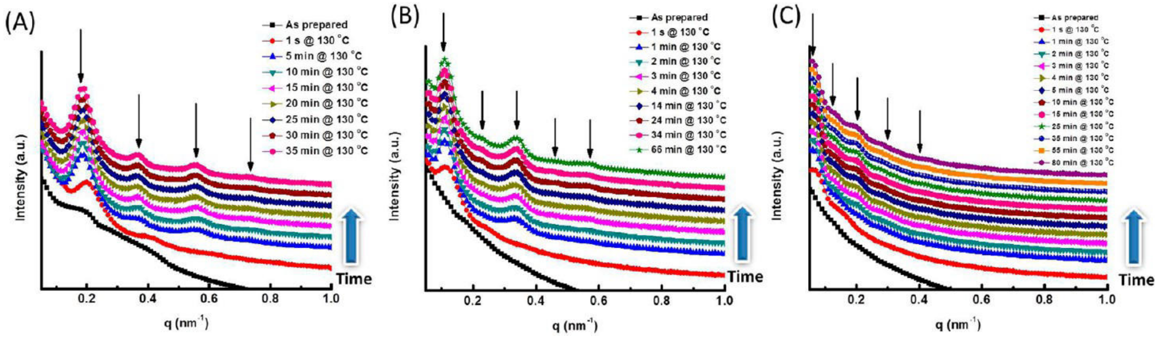

Figure 3-12. *In situ* SAXS of sample (A) [g-S$_{2.4}$]$_{35}$-b-[g-LA$_{2.4}$]$_{43}$, (B) [g-S$_{2.4}$]$_{51}$-b-[g-LA$_{2.4}$]$_{67}$, and (C) [g-S$_{2.4}$]$_{98}$-b-[g-LA$_{2.4}$]$_{124}$.

CONCLUSION AND FUTURE DIRECTIONS

In summary, symmetric brush BCPs of PLA and PS side chains self-assemble rapidly into highly ordered lamellar domains ranging from 20 to 235 nm, as revealed by SAXS, both in bulk and thin films. The domain size increases approximately linearly with the DP of the backbone, which indicates that the backbone is in an extremely extended conformation. The domain spacing was found to be consistently larger in thin films than in bulk samples, and this was attributed to the swollen domains being kinetically trapped during the evaporation of the solvent vapor after the sample is removed from the annealing jar.

Further analysis of the higher MW samples (group III and group IV) is still underway, but preliminary results suggest that it may be more difficult to obtain well-ordered microdomains as the side chain size increases. Samples have also been synthesized with a few units of deuterated PS (PS(*d*8)) side chains at the end of the brush BCP for small-angle neutron scattering (SANS) studies (**Table 3-3**). The SANS studies will be used to provide evidence to distinguish if these brush polymers undergo a normal head-to-head packing or if they undergo interdigitate packing (**Scheme 3-3**).

Table 3-3. Characteristics of brush BCPs with deuterated PS at the end of the brush BCP.

Sample	M_n [a] (× 10^3 g/mol)	PDI [a]	DP - PLA [b]	DP - PS [c]	DP - PS(*d*8) [d]	Total DP
1	417	1.02	44	40	5	89
2	862	1.03	91	83	9	183
3	1794	1.10	190	172	20	382

[a] Determined by THF GPC using RI and MALLS detectors. [b] DP of the PLA MM (M_n = 4.76 ×10^3 g/mol) as estimated by GPC and mol % of MM used during ROMP. [c] DP of the PS MM (M_n = 4.67 ×10^3 g/mol) as estimated by GPC and mol % of MM used during ROMP. [d] DP of the PS(*d*8) MM (M_n = 4.69 ×10^3 g/mol) as estimated by GPC and mol % of MM used during ROMP.

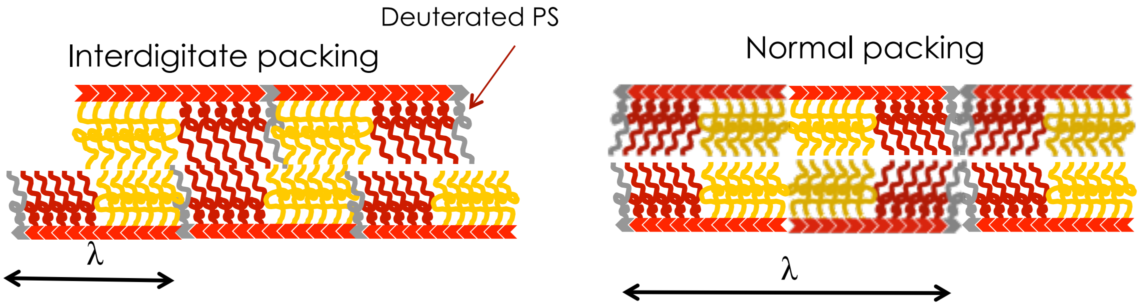

Scheme 3-3. A schematic illustration of the expected self-assembly of brush BCPs with deuterated PS side chains at the end, undergoing either interdigitate packing (left) or normal packing (right).

REFERENCES:

(1) Park, M.; Harrison, C.; Chaikin, P. M.; Register, R. A.; Adamson, D. H. *Science* **1997**, *276*, 1401.

(2) Li, R. R.; Dapkus, P. D.; Thompson, M. E.; Jeong, W. G.; Harrison, C.; Chaikin, P. M.; Register, R. a.; Adamson, D. H. *Appl. Phys. Lett.* **2000**, *76*, 1689.

(3) Thurn-Albrecht, T.; Schotter, J.; Kastle, G. A.; Emley, N.; Shibauchi, T.; Krusin-Elbaum, L.; Guarini, K.; Black, C. T.; Tuominen, M. T.; Russell, T. P. *Science* **2000**, *290*, 2126.

(4) Kim, B. H.; Jia, X.; Stafford, C. M.; Kim, D. H.; Mccarthy, T. J.; Tuominen, M.; Hawker, C. J.; Russell, T. P. *Adv. Mater.* **2001**, *13*, 795.

(5) Cheng, J. Y.; Ross, C. A.; Chan, V. Z.; Thomas, E. L.; Lammertink, R. G. H.; Vancso, G. J. *Adv. Mater.* **2001**, *13*, 1174.

(6) Black, C. T.; Guarini, K. W.; Milkove, K. R.; Baker, S. M.; Russell, T. P.; Tuominen, M. T. *Appl. Phys. Lett.* **2001**, *79*, 409.

(7) Lopes, W. a; Jaeger, H. M. *Nature* **2001**, *414*, 735.

(8) Black, C. T. *Appl. Phys. Lett.* **2005**, *87*, 163116.

(9) Pelletier, V.; Asakawa, K.; Wu, M.; Adamson, D. H.; Register, R. a.; Chaikin, P. M. *Appl. Phys. Lett.* **2006**, *88*, 211114.

(10) Cheng, J. Y.; Ross, C. a.; Smith, H. I.; Thomas, E. L. *Adv. Mater.* **2006**, *18*, 2505.

(11) Kang, Y.; Walish, J. J.; Gorishnyy, T.; Thomas, E. L. *Nat. Mater.* **2007**, *6*, 957.

(12) Luttge, R. *J. Phys. D Appl. Phys.* **2009**, *42*, 123001.

(13) Xu, J.; Hong, S. W.; Gu, W.; Lee, K. Y.; Kuo, D. S.; Xiao, S.; Russell, T. P. *Adv. Mater.* **2011**, *23*, 5755.

(14) Gu, X.; Liu, Z.; Gunkel, I.; Chourou, S. T.; Hong, S. W.; Olynick, D. L.; Russell, T. P. *Adv. Mater.* **2012**, *24*, 5688.

(15) Bates, F. S.; Fredrickson, G. H. *Annu. Rev. Phys. Chem.* **1990**, *41*, 525.

(16) Hamley, I. W. *Nanotechnology* **2003**, *14*, R39.

(17) Park, C.; Yoon, J.; Thomas, E. L. *Polymer* **2003**, *44*, 6725.

(18) Segalman, R. A. *Mater. Sci. Eng. R Rep.* **2005**, *48*, 191.

(19) Stoykovich, M. P.; Nealey, P. F. *Nature* **2006**, *9*, 20.

(20) Park, S.; Lee, D. H.; Xu, J.; Kim, B.; Hong, S. W.; Jeong, U.; Xu, T.; Russell, T. P. *Science* **2009**, *323*, 1030.

(21) Marencic, A. P.; Register, R. A. *Annu. Rev. Chem. Biomol. Eng.* **2010**, *1*, 277.

(22) Albert, J. N. L.; Epps, T. H. *Mater. Today* **2010**, *13*, 24.

(23) Tseng, Y.-C.; Darling, S. B. *Polymers* **2010**, *2*, 470.

(24) Gedde, U. F. *Polymer Physics*; Springer: London, 1995.

(25) RamachandraRao, V. S.; Gupta, R. R.; Russell, T. P.; Watkins, J. J. *Macromolecules* **2001**, *34*, 7923.

(26) Kim, E.; Ahn, H.; Park, S.; Lee, H.; Lee, M.; Lee, S.; Kim, T.; Kwak, E.-A.; Lee, J. H.; Lei, X.; Huh, J.; Bang, J.; Lee, B.; Ryu, D. Y. *ACS Nano* **2013**, *7*, 1952.

(27) Fink, Y.; Urbas, A. M.; Bawendi, M. G.; Joannopoulos, J. D.; Thomas, E. L. *J. Light. Technol.* **1999**, *17*, 1963.

(28) Kang, C.; Kim, E.; Baek, H.; Hwang, K.; Kwak, D.; Kang, Y.; Thomas, E. L. *J. Am. Chem. Soc.* **2009**, *131*, 7538.

(29) Yoon, J.; Mathers, R. T.; Coates, G. W.; Thomas, E. L. *Macromolecules* **2006**, *39*, 1913.

(30) Runge, M. B.; Dutta, S.; Bowden, N. B. *Macromolecules* **2006**, *39*, 498.

(31) Rzayev, J. *Macromolecules* **2009**, *42*, 2135.

(32) Oono, Y.; Bahiana, M. *Phys. Rev. Lett.* **1988**, *61*, 1100.

(33) Zalusky, A. S.; Olayo-Valles, R.; Wolf, J. H.; Hillmyer, M. A. *J. Am. Chem. Soc.* **2002**, *124*, 12761.

(34) Delamarche, E.; Michel, B.; Gerber, C.; Anselmetti, D.; Guntherodt, H.-J.; Wolf, H.; Ringsdorf, H. *Langmuir* **1994**, *10*, 2869.

(35) Mansky, P.; Liu, Y.; Huang, E.; Russell, T. P.; Hawker, C. *Science* **1997**, *275*, 1458.

(36) Ryu, D. Y.; Shin, K.; Drockenmuller, E.; Hawker, C. J.; Russell, T. P. *Science* **2005**, *308*, 236.

(37) Ji, S.; Liu, C.-C.; Son, J. G.; Gotrik, K.; Craig, G. S. W.; Gopalan, P.; Himpsel, F. J.; Char, K.; Nealey, P. F. *Macromolecules* **2008**, *41*, 9098.

(38) Russell, T. P.; Coulon, G.; Deline, V. R.; Miller, D. C. *Macromolecules* **1989**, *22*, 4600.

(39) Anastasiadis, S. H.; Russell, T. P.; Satija, S. K.; Majkrzak, C. F. *J. Chem. Phys.* **1990**, *92*, 5677.

(40) Hu, M.; Xia, Y.; McKenna, G. B.; Kornfield, J. A.; Grubbs, R. H. *Macromolecules* **2011**, *44*, 6935.